



Open Research Online

The Open University's repository of research publications and other research outputs

Penetrometry of granular and moist planetary surface materials: Application to the Huygens landing site on Titan

Journal Item

How to cite:

Atkinson, Karl R.; Zarnecki, John C.; Towner, Martin C.; Ringrose, Timothy J.; Hagermann, Axel; Ball, Andrew J.; Leese, Mark R.; Kargl, Gunter; Paton, Mark D.; Lorenz, Ralph D. and Green, Simon F. (2010). Penetrometry of granular and moist planetary surface materials: Application to the Huygens landing site on Titan. *Icarus*, 210(2) pp. 843–851.

For guidance on citations see [FAQs](#).

© 2010 Elsevier Inc

Version: Accepted Manuscript

Link(s) to article on publisher's website:

<http://dx.doi.org/doi:10.1016/j.icarus.2010.07.019>

Copyright and Moral Rights for the articles on this site are retained by the individual authors and/or other copyright owners. For more information on Open Research Online's data [policy](#) on reuse of materials please consult the policies page.

oro.open.ac.uk

1 **Penetrometry of granular and moist planetary surface materials:**

2 **Application to the Huygens landing site on Titan**

3

4 Karl R. Atkinson^a, John C. Zarnecki^a, Martin C. Towner^{a,1}, Timothy J. Ringrose^a, Axel
5 Hagermann^a, Andrew J. Ball^{a,2}, Mark R. Leese^{a,*}, Gunter Kargl^b, Mark D. Paton^{a,3}, Ralph D.
6 Lorenz^{c,a} and Simon F. Green^a

7

8 ^a PSSRI, The Open University, Walton Hall, Milton Keynes, MK7 6AA, U.K.

9 ^b Space Research Institute, Austrian Academy of Sciences, Schmiedlstraße 6, A-8042 Graz-
10 Messendorf, Austria.

11 ^c Space Department, Johns Hopkins University Applied Physics Laboratory, 111100 Johns
12 Hopkins Road, Laurel, MD 20723-6099, USA.

13

14 ¹ Present address: Impacts and Astromaterials Research Centre (IARC), Earth Sciences and
15 Engineering Department, Imperial College London, South Kensington, London, SW7 2AZ, UK.

16 ² Present address: European Space Research & Technology Centre, Keplerlaan 1, Postbus 299,
17 2200 AG Noordwijk, The Netherlands.

18 ³ Present address: P.O.Box 64 (Gustaf Hällströmin katu 2a), FI-00014 University of Helsinki,
19 Helsinki, Finland.

20

21 Number of pages: 42

22 Number of Figures: 13

23 Number of Tables: 1

24 Proposed Running Head:

25 Penetrometry of Titan Surface

26

27 *Corresponding author:

28 Mark Leese

29 PSSRI, The Open University, Walton Hall, Milton Keynes, MK7 6AA, U.K.

30 Tel +44 (0)1908 652561

31 Fax: +44 (0)1908 858022

32 e-mail: m.r.leese@open.ac.uk

33

34 e-mails:

35 Karl R. Atkinson: fluid.aspect@gmail.com

36 John C. Zarnecki: j.c.zarnecki@open.ac.uk

37 Martin C. Towner: m.towner@ic.ac.uk

38 Timothy J. Ringrose: t.j.ringrose@open.ac.uk

39 Axel Hagermann: a.hagermann@open.ac.uk

40 Andrew J. Ball: Andrew.ball@esa.int

41 Mark R. Leese: m.r.leese@open.ac.uk

42 Gunter Kargl: guenter.kargl@oeaw.ac.at

43 Mark D. Paton: mark.paton@helsinki.fi

44 Ralph D. Lorenz: ralph.lorenz@jhuapl.edu

45 Simon F. Green: s.f.green@open.ac.uk

46 **Abstract**

47 The Huygens probe landed on the then unknown surface of Titan in January 2005. A
48 small, protruding penetrometer, part of the Surface Science Package (SSP), was pushed into the
49 surface material measuring the mechanical resistance of the ground as the probe impacted the
50 landing site. We present laboratory penetrometry into room temperature surface analogue
51 materials using a replica penetrometer to investigate further the nature of Titan's surface and
52 examine the sensor's capabilities. The results are then compared to the flight instrument's
53 signature and suggest the Titan surface substrate material consists of sand-sized particles with a
54 mean grain size ~ 2 mm. A possible thin 7 mm coating with mechanical properties similar to
55 terrestrial snow may overlie this substrate, although due to the limited data we are unable to
56 detect any further layering or grading within the near-surface material. The unusual weakening
57 with depth of the signature returned from Titan has, to date, only been reproduced using a damp
58 sand target that becomes progressively wetter with depth, and supports the suggestion that the
59 surface may consist of a damp and cohesive material with interstitial liquid contained between its
60 grains. Comparison with terrestrial analogues highlights the unusual nature of the landing site
61 material.

62

63 *Keywords:* Titan; Regoliths; Ices, mechanical properties

64 **1 Introduction**

65 On the 14th January 2005, the Huygens probe successfully completed the first landing on
66 the unexplored surface of Titan (Lebreton *et al.* 2005). The probe and Cassini orbiter have since
67 revealed the Titan surface to consist of a wide range of geological features including sand dunes,
68 lakes, mountain chains and dendritic channel networks (Coustenis and Hirtzig, 2009; Jaumann *et*
69 *al.*, 2008). The probe's scientific instrumentation included the Surface Science Package (SSP)
70 (Zarnecki *et al.*, 1997; Zarnecki *et al.*, 2002), a suite of small sensors primarily aimed at
71 characterising the nature of any solid or possibly liquid surface. This instrument included a
72 penetrometer, designated 'ACC-E' or ACCelerometer-External for historical reasons, as part of
73 its array of sensors. The original intention of the penetrometer was to provide a qualitative
74 identification of a terrestrial analogue material for Titan's surface in the event of a (soft) solid
75 landing (Lorenz *et al.*, 1994). The penetrometer was designed to measure forces ranging from a
76 few newtons up to a limit of 2000 N. Impact loads any higher than this would probably have
77 caused a failure of the probe (Lorenz *et al.*, 1994). No scientific return was expected from the
78 penetrometer in the case of a liquid landing due to the force on the tip being less than the trigger
79 threshold of the sensor (Zarnecki *et al.*, 1997). Additional design details are given in Krysinski *et*
80 *al.* (2009).

81

82 **2 Flight sensor and surface signature**

83 [Insert Fig. 1 here]

84 The ACC-E penetrometer consists of a piezoelectric element sandwiched between a 14
85 mm diameter hemispherical tip and collar, mounted at the end of a short aluminium pylon (Fig.
86 1). This element generates a charge proportional to the stress placed on it, thereby acting as a
87 force transducer allowing a direct measurement of the mechanical resistance of the material

88 encountered. Constraints were placed on the positioning and length of the flight penetrometer due
89 to the crystal being located directly behind the probe's heat shield (Lorenz *et al.*, 1994). For
90 electromagnetic compatibility, a mesh screen, through which the penetrometer passed, covered
91 the base of the SSP instrument. The electronics were designed to sample the sensor at a rate of 10
92 kHz such that at the expected impact speed on Titan of 5 m s^{-1} , a theoretical depth resolution of 1
93 mm might be obtained. This resolution was intended to allow the possibility of identifying
94 layering in the surface or particle size if the material was granular. The probe landed slightly
95 slower than this at $4.60 \pm 0.05 \text{ m s}^{-1}$ (Towner *et al.*, 2006; Zarnecki *et al.*, 2005). For an impact
96 under parachutes at this constant vertical speed, the penetrometer force signature can be plotted
97 against depth penetrated as shown in Fig. 2.

98 [insert Fig. 2 here]

99 This signature can be considered in four distinct stages; however for the purposes of this
100 analysis only the first three stages are useful, before the addition of strong structural interactions
101 caused by the arrival of the probe foredome at the surface that make the later data (stage 4)
102 unusable. The first stage is a weak but rising force corresponding to a material thickness of 7-8
103 mm. The second stage is a sudden resistance spike of less than 1 ms duration, equivalent to $\sim 2\text{-}3$
104 mm penetration depth at the 4.6 m s^{-1} impact speed. This is followed by the longest period of
105 'clean' penetration before an abrupt rise in force seen in stage 4 which corresponds with the
106 arrival of the Electromagnetic Compatibility (EMC) screen of the Surface Science Package some
107 55 mm after penetrometer tip entry (Zarnecki *et al.*, 2005). The pre-impact signature by design
108 showed 64 force samples before the triggering threshold. Due to shorter, fixed wiring and better
109 screening, noise levels are lower than those measured with the laboratory equipment, occupying

110 only the least significant bit level of the 8 bit analogue to digital converter (ADC) of the SSP
111 electronics, equivalent to a force of 2 N at Titan surface temperature.

112

113 **3 Analogue work**

114 Using a replica ACC-E penetrometer and a portable test rig with an electromagnetic
115 release, penetrometry drops were carried out at the probe impact speed both in the laboratory and
116 in the field (for a summary of drops presented in this paper see Table 1). To produce drops
117 comparable to that made by the 200.5 kg probe on Titan, it is only necessary to attach the
118 penetrometer to a small 5 kg mass that provides sufficient inertia to maintain the impact speed for
119 the duration of penetration (Lorenz *et al.*, 1994). The required impact speed was achieved by
120 adjusting the height of the drop, equating the gravitational potential energy lost with the kinetic
121 energy on impact assuming negligible drag. The impact speed for each drop was verified using a
122 laser, photodiode sensor array, and barcode etched mirror attached to the penetrometer weight
123 (Fig. 3). For a fuller description see Atkinson (2008).

124 The penetrometry in the laboratory was intended to produce impact signatures
125 representative of similar impacts into a semi-infinite planetary surface. In practice, a laboratory
126 target is necessarily bounded by the rigid sidewalls of the target container and the depth restricted
127 by the container floor. Boundaries may lead to spurious effects on the penetrometer signal caused
128 by the confinement and induced order in the target material near the container wall (Zou and Yu,
129 1995). This leads to a compromise between as large a target as possible, to minimise these
130 effects, and the practicality of producing a target that is manageable in size and not too time
131 consuming to prepare. Boundary effects have been examined extensively and various ‘correction
132 factors’ have been proposed to account for the effects with varying degrees of success (see e.g.
133 Huang and Hsu, 2005).

134 An analysis of boundary effects is beyond the scope of this study as the effect can be
135 dependent on multiple factors including the type of target material, its preparation, and the
136 sensitivity of the penetrometer. For the purposes of the analogue experiments however, it was not
137 necessary to examine the boundary effects *per se*, but only to establish a target container size of
138 sufficient dimension for them to be negligible. This was done by comparison of the mean force
139 detected between multiple sets of drops into cylindrical targets of varying diameter and depth.
140 The target material was chosen to be 4mm diameter
141 spherical glass beads, as these pack consistently to a narrow range of bulk density, and are easily
142 prepared by pouring. To examine edge effects, three open-bottomed cylindrical containers of
143 internal diameters 104, 152 and 235 mm were placed within a larger 320 mm diameter closed-
144 bottomed cylindrical container. All four containers were filled with glass beads to a depth of 350
145 mm. Ten drops were carried out into each size container and the mean signature force recorded.
146 Using a one-way analysis of variance (ANOVA) followed by a Tukey Honestly Significant
147 Difference (HSD) multiple comparison test (see e.g. LeBlanc, 2004), a statistically significant
148 increase in mean signature force was measured between the smallest diameter container and the
149 other three containers. To test the effect of the container floor, the 235 mm diameter open-
150 bottomed cylindrical container was set on increasing levels of Foamglas, a rigid but brittle
151 cellular glass insulating material that would crush, avoiding damage to the penetrometer should it
152 not be stopped by the beads. This produced targets of four depths: 350 mm (no Foamglas), 270,
153 190 and 110 mm respectively. A similar ANOVA and multiple comparison test analysis found
154 the mean penetration force experienced when using the small 110 mm depth container was
155 significantly higher than for the other three containers. These results implied a minimum target
156 container size of ~152 mm diameter and 190 mm depth was needed for boundary effects to be

157 considered negligible. Based on these results, for most experiments the largest container (320 mm
158 diameter, 350 mm depth) was used.

159 [Insert Table 1 here]

160

161 **4 Signal processing path and sensor calibration**

162 The penetrometer front-end electronics consists of a charge amplifier followed by a
163 pseudo-logarithmic amplifier used to accommodate the large range of input signals that could be
164 generated from the possible impact forces. This pseudo-logarithmic amplifier has three linear
165 gain branches selected depending on the input voltage. In the case of the flight data, only the
166 high-gain branch of this amplifier was used, as the force on the penetrometer was at the low
167 (softer impact) end of the range. An anti-aliasing filter is used to remove frequencies above the
168 sensor's Nyquist frequency (5 kHz) before an 8-bit Analogue to Digital converter (ADC). Figure
169 3 summarises the signal processing paths for the flight and laboratory data.

170 [Insert Fig. 3 here]

171 The replica penetrometer was made using a piezoelectric crystal from the same batch as
172 the flight and flight spare penetrometers and constructed in accordance with the original assembly
173 instructions. The charge generated by the piezoelectric crystal leaks away rapidly after the
174 application of a force to the penetrometer tip. For this reason, it is not possible to calibrate the
175 crystal by applying static loads- a known dynamic force must be used instead (Lorenz *et al.*,
176 1994; Zarnecki *et al.*, 1997). The original ACC-E penetrometers were calibrated using a small
177 pendulum jig to strike the sensor tip with different impactors (Lorenz 1994a; Lorenz *et al.*, 1994).
178 For the replica penetrometer, a different method was used based on a mass moving on a
179 frictionless horizontal linear bearing colliding with the force transducer (Fujii, 2006; Fujii and
180 Fujimoto, 1999). This highly accurate calibration method used an optical interferometer to

181 determine the change in momentum of the moving mass before and after the collision. This
182 change is equal in magnitude to the time integrated impulse acting on a force transducer. Given
183 that this degree of calibration accuracy was not required for the penetrometer, the interferometer
184 was replaced with a suitable accelerometer which allowed a direct determination of the impact
185 force for a known impact mass. The limitations of impacting mass that could be supported on the
186 frictionless linear track used meant only the high gain branch was calibrated. Piezoelectric crystal
187 sensitivity varies with temperature and therefore a conversion factor of 1.83 (Lorenz *et al.*, 1994)
188 was required to account for the reduction in sensitivity of the flight signature returned from
189 Titan's -180°C surface compared to the room temperature analogue signatures.

190

191 **5 Identifying substrate material grain size**

192 Grain size is of key interest to the Huygens penetrometry investigation due to the strong
193 indication of a sedimentary granular environment at the landing site (Tomasko *et al.*, 2005). One
194 approach to this type of investigation has attempted to reconstruct the grain size distributions of
195 Martian soil analogues from their quasi-static penetrometry signatures by examining frequency
196 content (Kargl *et al.*, 2009). The limitations imposed by the length, the relatively low sampling
197 rate of the ACC-E penetrometer and higher speed of impact meant this technique could not be
198 applied. An alternative method was used to examine laboratory penetrometry drops collected at
199 the probe's impact speed into targets of glass and plastic spherical beads of known material
200 densities and with diameters between 1 and 8 mm. The amplitude of each peak in the resulting
201 signatures was identified after discarding peaks due to signal noise determined by examining the
202 pre-impact signal. First, to ensure the data were stationary, a moving average was subtracted from
203 each signature. The signature data points were then stepped through and all consecutive rises

204 between sample points summed until a falling value was found. If the sum of the rises was
205 greater than a 95% confidence level of the pre-impact signal (i.e. peak to trough as the
206 penetrometer is falling towards the target), the peak was considered significant and the point was
207 marked as a peak candidate. For this value to be accepted as a peak, an equivalent fall or sum of
208 consecutive falls must follow this candidate point. A similar method was used to find trough
209 candidates (Fig. 4). The mean value of peak to trough height for each target was then determined.

210 [Insert Fig. 4 here]

211 During this analysis, a regular enhancement of the penetration force in the first 8-10 mm
212 of target penetration or ‘tip entry effect’ was evident that considerably affected the mean peak to
213 trough height and variability. This distance corresponds approximately to the length of the ACC-
214 E hemispherical tip as it enters the target surface. In general, the effect was found to be greater
215 for larger beads. One possible explanation is given by comparison of the size of the penetrometer
216 tip to the target beads. Smaller bead targets present more of a smooth continuum surface to the tip
217 with each bead having proportionately less effect on it. However, large beads whose size is
218 comparable to the tip form an uneven target surface with variations in both the number and
219 position of the beads impacted. After the tip has fully entered the target it is completely
220 surrounded and therefore gives a more uniform response. Figure 5 shows the magnitude of the
221 mean peak to trough force plotted against the bead mass after removal of the ‘tip entry effect’.

222 [Insert Fig. 5 here]

223 A statistically significant empirical relationship between bead mass and the mean peak-
224 trough amplitude, h , was found:

225
$$h = 37.79M^{0.33} \quad (1)$$

226

227 **6 Substrate material properties with depth**

228 The third stage (Fig. 2) of the flight signature lasts 8.3 ms and is unusual due to a
229 significant downward trend; resistance usually increases as the target material becomes
230 compacted in front of the advancing penetrometer, and/or overburden pressure increases the
231 penetration resistance. Several analogues were tested to try to reproduce this trend. One
232 possibility, given the fluvial nature of the surface seen in DISR images, was that the granular
233 material could be size sorted with depth, which might affect the resistance. This effect, known as
234 graded bedding, is due to changes in the flow speed of the liquid transporting the grains and can
235 result in either ‘normal grading’, where the grain size coarsens with depth, or ‘inverse grading’
236 where the material becomes finer with depth.

237 Artificial graded targets were produced with layers of the four sizes of available glass
238 beads (8, 6, 4 and 1 mm diameter). Whilst some of the inverse graded drops had a downward
239 trend the gradients varied too much to be pursued as a suitable analogue.

240 Further attempts to reproduce a downward trend using clay targets with added voids were
241 only partially successful in modifying the typically flat clay signature to a slightly downward-
242 sloped one. The gradient of the Titan signature is significantly greater over a short length than
243 seen in a clay void target. Early material catalogue work had shown that some water-wetted sand
244 targets were able to produce a downward signature slope although the amount and distribution of
245 liquid had not been well characterized (Paton, 2005). Examining the effect of water on
246 penetration resistance in soils is often done using penetrometers with combined Time Domain
247 Reflectometry (TDR) probes that measure soil water content *in situ* as they penetrate the soil (see
248 e.g., Vaz *et al.*, 2001). The ACC-E did not have this capability; however by using a ThetaProbe
249 (Delta-T, 1999) to measure the moisture through small sampling points in the target container
250 wall, water distribution could be determined immediately prior to penetrometer impact with

251 minimal target disturbance. Sand targets were prepared in a rigid plastic cylindrical container
252 (diameter 320 mm and sand surface at 350 mm) using a similar method to that used in an
253 investigation to measure elastic wave velocities in saturated sand (Velea *et al.*, 2000). Two target
254 materials were used: well-sorted coarse grained Leighton Buzzard DA 16/30 sand (median grain
255 size, $D_{50} = 614 \mu\text{m}$) and well-sorted fine grained RH T sand ($D_{50} = 230 \mu\text{m}$) both locally
256 sourced from the WBB Minerals Ltd., Double Arches quarry in Leighton Buzzard, U.K.. The
257 sand targets were poured loosely in the container giving approximate dry bulk densities of 1.51
258 and 1.57 g cm^{-3} for the LB DA 16/30 and RH T sand respectively. To make a reproducible wet
259 target, water from an external feed bottle was introduced into the sand from below through a
260 perforated hose by capillary action causing minimal disturbance to the sand. The sand was
261 allowed to saturate completely to ensure even settlement and a glass straw (open to the
262 atmosphere) in the feed bottle was set at the required water table level. The sand was then
263 allowed to dry overnight until air in the straw of the feed bottle started bubbling up. At this point,
264 the water table is level with the bottom of the straw in the feed bottle. This produces, by capillary
265 action, a moisture gradient between the water table and the surface that can be controlled by
266 adjusting the depth of water table from the surface (or equivalently its height from the fixed
267 bottom of the target container). Immediately prior to the drop into the target, the water content
268 was sampled at several points along the height of the container using the ThetaProbe that after
269 calibration gave a DC voltage related to the soil water moisture content. Figure 6 illustrates the
270 experimental arrangement used.

271 [Insert Fig. 6 here]

272 Drops were carried out into both sands with four water table configurations, at $z=150$,
273 200, 250 and 350 mm (saturated sand) where z is the height of the water table measured from the

274 bottom of the target container. Due to the time-consuming target preparation and subsequent
275 necessity to allow each sand to dry completely before it could be used to prepare a new target,
276 only four drops were carried out into each of the two sands. For comparison with the wet sand
277 signatures, several drops were also carried out into the two dry sands at loose and dense
278 compaction states. Representative signatures from these drops are shown in Fig. 7 and Fig. 8.

279 [Insert Fig. 7 here]

280 [Insert Fig. 8 here]

281 The coarser grained LB sand has a higher penetration resistance than the finer RH T sand
282 and, as expected, the compacted state of each sand type has greater mechanical strength than the
283 loose state. Once water is introduced into these sands even in small quantities, their penetrometry
284 signatures change considerably. Figure 9 shows the RH T sand signatures for the four
285 configurations tested. With the exception of the drop into sand with the lowest water table (d), the
286 characteristic dry sand shape is not seen; the initial tip entry peak of the sand has gone. The other
287 signatures are similar to that of cohesive clay, with a gradual rising slope followed by an
288 essentially constant resistance plateau. This plateau seems to vary in force depending on the
289 height of the water table. The saturated sand, (a), has the lowest resistance, only slightly higher
290 than that of the same sand when dry and in a loosely packed state (Fig. 7). In contrast, the sand
291 with the lowest water table at $z=150$ mm, (d), has a much greater resistance with a plateau phase
292 nearly twice that of the same sand in the dry dense state. The tip entry peak also returns in this
293 signature. The entry rise of each signature also varies with the moisture content of the sand. The
294 sand with the lowest water table and therefore driest surface, (d), has the sharpest rising force. As
295 the water table is raised and the moisture content of the sand near the surfaces increases, this
296 entry rise becomes increasingly gradual.

297 [Insert Fig. 9 here]

298 Coarser LB sand in the same wet drop configurations produces different results (Fig. 10).
299 A drop into saturated sand (a) shows a considerably reduced tip entry peak compared with drops
300 into the same sand when dry, followed by a constant resistance plateau similar to that seen in the
301 wet RH T sand. In subsequent drops, (b) and (c), as the water level is lowered the initial tip entry
302 peak increases in resistance but falls gradually producing a downward gradient similar to that
303 seen in the Huygens signature. Finally, in drop (d) with the saturation level 200 mm below the
304 target surface, the sand starts to behave as if in the dry state again, with a slightly more
305 pronounced tip-entry peak and a gradual increase in resistance with depth in the plateau phase.
306 These signatures again show how the addition of small quantities of water between the grains of
307 sand can modify the penetrometry signature even over a short penetration distance and, in some
308 cases, more than double the average penetration resistance compared to the same sand in the dry
309 state.

310 [Insert Fig. 10 here]

311

312 **7 Comparison of laboratory analogue results to the Huygens landing site signature**

313 The laboratory analogue penetrometry work can be compared with the signature returned
314 by the ACC-E penetrometer from the Huygens landing site and some of the findings described
315 previously can be applied. Although the first two stages of the flight data are of extremely short
316 duration, the closest match suggests that the penetrometer's first contact with the surface may
317 have been into a thin coating on the substrate material with weaker mechanical properties than
318 terrestrial snow (Fig. 11). At a 4.6 m s^{-1} impact speed, this putative coating has a thickness of
319 $\sim 7 \text{ mm}$. One possibility is that this layer is a loose covering of deposited atmospheric aerosols and
320 tholins. However, recent models of Titan's atmosphere indicate a surface deposition rate of 0.01
321 $\mu\text{m yr}^{-1}$ (Soderblom *et al.*, 2007), which would suggest that this coating has been deposited over

322 a period greater than 700,000 years. This would seem to be at odds with the current picture of a
323 dynamic Titan surface at the Huygens Landing site. Alternative origins for this layer may be
324 aeolian or fluvial in nature.

325 [Insert Fig. 11 here]

326 In previous analogue work (Zarnecki *et al.*, 2005), the force spike seen in the second stage
327 was reproduced by impacts with small pebbles or with hard crusts; however, the images of the
328 surface taken with the DISR cameras suggest a surface shaped by fluvial processes (Tomasko *et*
329 *al.*, 2005) with rounded pebbles 10-15 cm in diameter lying on top of a darker, grainy substrate
330 material, making an impact with the first of these analogues seem more likely.

331 Although the presence of water ice at the Titan landing site has yet to be confirmed
332 (Keller *et al.*, 2008), impacts at the Huygens speed were carried out into spherical water ice
333 particles of various masses frozen in liquid nitrogen, to reproduce the peak seen in stage 2 of the
334 Titan signature. While not conclusive, due to the difficulty in controlling the exact point of
335 impact between the penetrometer and ice particle, two drops into the smallest mass particle (~2g)
336 produced a signature peak of similar magnitude to that seen in the signature. This mass
337 corresponds to a spherical particle of approximately 16 mm in diameter, far smaller than the
338 scattered pebbles imaged on the surface by the DISR camera. Given that the accelerometer on the
339 SSP registered a small precursor peak of approximately 0.6 g in magnitude prior to the
340 penetrometer triggering, this would suggest that the probe foredome may have impacted a larger
341 pebble before the first contact of the penetrometer with a granule from the substrate material.

342 The downward pointing DISR Medium Resolution Imager (MRI) also separately imaged
343 the granular substrate material. Due to the limiting resolution of this imager, the smallest size of
344 grain that can be measured from the images is 3 mm. However, applying the results of the
345 laboratory bead drops, that the grain mass affects the amplitude of the peaks, an estimate of the

368 [Insert Fig. 13 here]

369 The identification map shows that even the closest terrestrial analogue match for this
370 substrate material, a gradient wetted coarse sand, while close to matching the mean peak-trough
371 undulations in the signature caused by granularity, is still some way from matching the degree of
372 loss of strength with depth. This cannot be explained by Titan's reduced gravity compared to
373 penetrometry drops carried out on Earth, as the flight data's signature gradient is negative.
374 Gravity acts to increase overburden pressure with depth and compress underlying material, which
375 would cause a positive signature gradient (and, for the small depth penetrated the effect of
376 overburden pressure would be negligible). It must be noted that these wet analogues used water
377 as their interstitial fluid, which at room temperature has a ~5 times greater viscosity and a surface
378 tension four times that of liquid methane on Titan's surface. Liquid methane at 95K has dynamic
379 viscosity of 2×10^{-4} Pa s and surface tension 0.018 N m^{-1} (Ghafoor and Zarnecki, 2000; Keller *et*
380 *al.*, 2008). On the other hand, the viscosity of liquid ethane at Titan surface temperatures is a little
381 higher than water (e.g. Lorenz *et al.*, 2010). Thus, while we acknowledge that fluid properties
382 and the currently unknown contact angle between water ice and liquid hydrocarbons at Titan
383 surface temperature may be different from those in our experiments, our analogue could in fact
384 be rather similar. Nevertheless, carrying out penetration experiments into ice particles mixed
385 with liquid methane/ethane under Titan's surface temperature and pressure conditions may help
386 constrain the quantity of liquid present between the grains. However, the cost and complexity of
387 producing a sufficiently large environmental chamber within which to perform such experiments
388 would be prohibitive.

389

390 **8 Other Huygens data that support the penetrometer findings**

391 That the substrate material was damp is supported by the measurement of a 40% increase
392 in the level of methane detected by the Gas Chromatograph Mass Spectrometer (GCMS) two
393 minutes after landing while the detection of nitrogen remained constant (Niemann *et al.*, 2005).
394 Modelling of the thermal environment of the inlet supports this possibility, indicating that the
395 heated inlet may have evaporated a small quantity of methane in the local material (Lorenz *et al.*,
396 2006). This suggests that liquid methane may be mixed with the surface material and was
397 evaporated by the GCMS inlet line heater until the liquid became depleted. Detection of a
398 possible dewdrop (Karkoschka and Tomasko, 2009) falling from the descent imager baffle is also
399 consistent with methane moisture being sweated out of the ground by the 20W surface science
400 lamp.

401 The Huygens probe overall endured a deceleration at impact of about 150 m s^{-2} (i.e. 15
402 Earth 'g'), the deceleration pulse lasting about 20 ms (Zarnecki *et al.*, 2005; Lorenz *et al.*, 2009).
403 Modelling (Lorenz, 1994b) established the range of target parameters over which the deceleration
404 would be sensitive to the target strength, rather than the deformation of the probe. Indeed, the
405 Huygens landing site was soft enough that probe deformation was minimal (although transient
406 structural 'ringing' is evident in some accelerometer data (Bettanini *et al.*, 2008)). Inspection of
407 the peak deceleration and the rise time of the pulse (Lorenz *et al.*, 2009) suggest that the surface
408 material averaged over the base of the probe ($\sim 1\text{m}^2$, as opposed to the $\sim 1\text{cm}^2$ of the penetrometer)
409 had some cohesion (i.e. bearing strength at zero penetration). This further supports the 'damp
410 sand' model discussed in the present paper. Dry sand has a rather longer rise time than was
411 observed.

412 Rock counts from the SLI imager (Keller *et al.*, 2008) identify a few gravel-sized particles
413 great than $\sim 5\text{mm}$ in the substrate material, although the majority of the material imaged is finer

414 than this. Nevertheless, sand at the landing site may have been rather coarse – Tomasko *et al.*
415 (2005) note that particles 3mm across (the limiting resolution of the camera) can be identified in
416 the post-impact images.

417

418 **9 Conclusions**

419 The ACC-E penetrometer made a single direct measurement of the mechanical properties
420 and texture of the surface material at the Huygens landing site. Comparative analysis of the
421 returned signature with those of terrestrial analogues taken together with measurements from
422 other instruments allows an interpretation of the surface material to be made. This work suggests
423 that the penetrometer is likely to have impacted a thin, extremely weak surface coating overlying
424 a small, hard substrate material granule before being driven into a coarse granular sand substrate
425 possibly wet with liquid methane.

426

427 **Acknowledgements**

428 KRA would like to acknowledge the receipt of a PPARC studentship under which this work was
429 carried out. JCZ and SFG acknowledge the financial support of The UK PPARC (now STFC)
430 (Grants ST/F003102/1 and PP/D000882/1). RDL acknowledges the support of NASA via the
431 Cassini Project at the Jet Propulsion Laboratory. MDP acknowledges the receipt of a Hosie
432 Bequest studentship from the Royal Astronomical Society.

433

434 **References**

435 Atkinson, K.R., 2008. Investigating the Physical Properties of Planetary Surfaces using the
436 Huygens Penetrometer. PhD Thesis, The Open University, Milton Keynes.

437 Bettanini, C., Zaccariotto, M. and Angrilli, F., 2008. Analysis of the HASI accelerometers data
438 measured during the impact phase of the Huygens Probe on the surface of Titan by means
439 of a simulation with a finite element model. *Planet. Space Sci.* 56, 715-727.

440 Collins, G.C., 2005. Relative rates of fluvial bedrock incision on Titan and Earth. (DOI
441 10.1029/2005GL024551). *Geophys. Res. Lett.* 32, L22202.

442 Coustenis, A. and Hirtzig, M., 2009. Cassini-Huygens results on Titan's surface. *Research in
443 Astronomy and Astrophysics* 9, 249-268.

444 Delta-T, 1999. *ThetaProbe Soil Moisture Sensor Type ML2x User Manual*. Cambridge: Delta-T
445 Devices Ltd.

446 Fujii, Y., 2006. Optical method for accurate force measurement: dynamic response evaluation of
447 an impact hammer. *Optical Engineering* 45, 2, 023002.

448 Fujii, Y. and Fujimoto, H., 1999. Proposal for an impulse response evaluation method for force
449 transducers. *Measurement Science and Technology* 10, N31-N33.

450 Ghafoor, N. and Zarnecki, J.C., 2000. Wind-driven surface waves on Titan. *J. Geophys. Res.* 105,
451 12,077-12,091.

452 Huang, A.B. and Hsu, H.H., 2005. Cone penetration tests under simulated field conditions.
453 *Geotechnique* 55, 345-354.

454 Jaumann, R., Brown, R.H., Stephan, K., Barnes, J.W., Soderblom, L.A., Sotin, C., Le Mouelic,
455 S., Clark, R.N., Soderblom, J., Buratti, B., Wagner, R., Mccord, T.B., Rodriguez, S.,
456 Baines, E.K., Cruikshank, D.P., Nicholson, P.D., Griffith, C.A., Langhans, M. and Lorenz,
457 R.D., 2008. Fluvial erosion and post-erosional processes on Titan. *Icarus* 197, 526-538.

458 Kargl, G., Zöhrer, A., Kömle, N.I. and Kaufmann, E., 2009. Reconstruction of grain size
459 distributions from quasi-satic soil penetrometry experiments. In: Kargl, G., Kömle, N.I.,

4 6 0 Ball, A.J. and Lorenz, R.D. (Eds.), Penetrometry in the Solar System II, 133-145. Austrian
4 6 1 Academy of Sciences Press, Vienna.

4 6 2 Karkoschka, E. and Tomasko, M., 2009. Rain and dewdrops on titan based on in situ imaging.
4 6 3 Icarus 199, 442-448.

4 6 4 Keller, H.U., Grieger, B., Küppers, M., Schröder, S.E., Skorov, Y.V. and Tomasko, M.G., 2008.
4 6 5 The properties of Titans surface at the Huygens landing site from DISR observations.
4 6 6 Planet. Space Sci. 56, 728-752.

4 6 7 Krysinski, Z.J., Zarnecki, J.C., Leese, M.R., Lorenz, R.D., Parker, D.J., Bannister, M., Sandford,
4 6 8 M., Delderfield, J., Daniell, P. and Jolly, H., 2009. Technical aspects of the Huygens SSP
4 6 9 penetrometer design, pp. 157-172 in Kargl, G., Kömle, N., Ball, A.J. and Lorenz, R.D. (Eds)
4 7 0 Penetrometry in the Solar System II, Austrian Academy of Sciences, Vienna.

4 7 1 Leblanc, D.C., 2004. Statistics: concepts and applications for science. Jones & Bartlett, London.

4 7 2 Lebreton, J.P., Witasse, O., Sollazzo, C., Blancquaert, T., Couzin, P., Schipper, A., Jones, J.B.,
4 7 3 Matson, D.L., Gurvits, L.I., Atkinson, D.H., Kazeminejad, B. and Pérez-Ayúcar, M., 2005.
4 7 4 An overview of the descent and landing of the Huygens probe on Titan. Nature 438, 758-
4 7 5 764.

4 7 6 Lorenz, R.D., 1994a. Exploring the surface of Titan. PhD thesis, University of Kent at
4 7 7 Canterbury.

4 7 8 Lorenz, R.D., 1994b. Huygens Probe Impact Dynamics, ESA Journal 18, 93-117.

4 7 9 Lorenz, R.D., Bannister, M., Daniell, P.M. and Krysinski, Z., Leese M.R. Miller R.J. Newton G.
4 8 0 Rabbetts P. Willett D.M. Zarnecki J.C. 1994. An impact penetrometer for a landing
4 8 1 spacecraft. Measurement Science and Technology 5, 1033-1041.

4 8 2 Lorenz, R. D., Newman, C. and Lunine, J.I., 2010. Threshold of wave generation on Titan's lakes
4 8 3 and seas: Effect of viscosity and implications for Cassini observations, Icarus, in press.

484 Lorenz, R.D., Niemann, H.B., Harpold, D.N., Way, S.H. and Zarnecki, J.C., 2006. Titan's damp
485 ground: Constraints on Titan surface thermal properties from the temperature evolution of
486 the Huygens GCMS inlet. *Meteoritics & Planetary Science* 41, 1705-1714.

487 Lorenz, R.D., Kargl, G., Ball, A.J., Zarnecki, J.C., Towner, M.C., Leese, M.R., McDonnell,
488 J.A.M., Atkinson, K.R., Hathi, B. and Hagermann, A. 2009. Titan surface mechanical
489 properties from the SSP ACC-I record of the impact deceleration of the Huygens probe, pp.
490 147-156 in Kargl, G., Kömle, N., Ball, A.J. and Lorenz, R.D. (Eds) *Penetrometry in the*
491 *Solar System II*, Austrian Academy of Sciences, Vienna.

492 Niemann, H.B., Atreya, S.K., Bauer, S.J., Carignan, G.R., Demick, J.E., Frost, R.L., Gautier, D.,
493 Haberman, J.A., Harpold, D.N., Hunten, D.M., Israël, G., Lunine, J.I., Kasprzak, W.T.,
494 Owen, T.C., Paulkovich, M., Raulin, F., Raaen, E. and Way, S.H., 2005. The abundances of
495 constituents of Titan's atmosphere from the GCMS instrument on the Huygens probe.
496 *Nature* 438, 779-784.

497 Paton, M.D., 2005. *Penetrometry of NEOs and other solar system bodies*. PhD Thesis, The Open
498 University, Milton Keynes.

499 Soderblom, L.A., Kirk, R.L., Lunine, J.I., Anderson, J.A., Baines, K.H., Barnes, J.W., Barrett,
500 J.M., Brown, R.H., Buratti, B.J., Clark, R.N., Cruikshank, D.P., Elachi, C. Janssen, M.A.,
501 Jaumann, R., Karkoschka, E., Le Mouélic, S., Lopes, R.M., Lorenz, R.D., McCord, T.B.,
502 Nicholson, P.D., Radebaugh, J., Rizk, B., Sotin, C., Stofan, E.R., Sucharski, T.L., Tomasko,
503 M.G. and Wall, S.D. 2007. Correlations between Cassini VIMS spectra and RADAR SAR
504 images: Implications for Titan's surface composition and the character of the Huygens
505 Probe Landing Site. *Planet. Space Sci.* 55, 2025–2036.

506 Tomasko, M.G., Archinal, B.A., Becker, T.L., Bezare, Bushroe, M.W., Combes, M., Cook, D.A.,
507 Coustenis, A., De Bergh, C., Dafoe, L.E., Doose, L.R., Douté, S., Eibl, A., Engel, S.,

508 Gliem, F., Grieger, B., Holso, K., Howington-Kraus, E., Karkoschka, E., Keller, H.U.,
509 Kirk, R.L., Kramm, R., Küppers, M., Lanagan, P., Lellouch, E., Lemmon, M.T., Lunine,
510 J.I., Mcfarlane, E.A., Moores, J., Prout, G.M., Rizk, B., Rosiek, M.R., Rueffer, P.,
511 Schröder, S.E., Schmitt, B., See, C., Smith, P.H., Soderblom, L.A., Thomas, N. and West,
512 R.A., 2005. Rain, winds and haze during the Huygens probe's descent to Titan's surface.
513 Nature 438, 765-778.

514 Towner, M.C., Garry, J.R., Lorenz, R.D., Hagermann, A., Hathi, B., Svedhem, H., Clark, B.C.,
515 Leese, M.R. and Zarnecki, J.C., 2006. Physical properties of Titans surface at the Huygens
516 landing site from the Surface Science Package Acoustic Properties sensor (API-S). Icarus
517 185, 457-465.

518 Vaz, C.M., Bassoi, L.H. and Hopmans, J.W., 2001. Contribution of water content and bulk
519 density to field soil penetration resistance as measured by a combined cone penetrometer-
520 TDR probe. Soil and Tillage Research 60, 35-42.

521 Velea, D., Shields, F.D. and Sabatier, J.M., 2000. Elastic Wave Velocities in Partially Saturated
522 Ottawa Sand: Experimental Results and Modeling. Soil Science Society of America Journal
523 64, 1226-1233.

524 Wentworth, C.K., 1922. A scale of grade and class terms for clastic sediments. Journal of
525 Geology 30, 377-392.

526 Zarnecki, J.C., Banaszkiwicz, M., Bannister, M., Boynton, W.V., Challenor, P.G., Clark, B.C.,
527 Daniell, P.M., Delderfield, J., English, M.A., Fulchignoni, M., Garry, J.R., Geake, J.E.,
528 Green, S.F., Hathi, B., Jaroslowski, S., Leese, M.R., Lorenz, R.D., McDonnell, J.A.M.,
529 Merryweather-Clarke, N., Mill, C.S., Miller, R.J., Newton, G., Parker, D.J., Rabbetts, P.,
530 Svedhem, H., Turner, R.F. and Wright, M.J., 1997. The Huygens Surface Science Package.
531 In: Wilson, A. (Ed.), Huygens. Science, Payload and Mission: European Space Agency.

- 532 Zarnecki, J.C., Leese, M.R., Garry, J.R., Ghafoor, N. and Hathi, B., 2002. Huygens' Surface
533 Science Package. *Space Science Reviews* 104, 591-609.
- 534 Zarnecki, J.C., Leese, M.R., Hathi, B., Ball, A.J., Hagermann, A., Towner, M.C., Lorenz, R.D.,
535 Mcdonnell, J.A.M., Green, S.F., Patel, M.R., Ringrose, T.J., Rosenberg, P.D., Atkinson, K.
536 R., Paton, M.D., Banaszkiwicz, M., Clark, B.C., Ferri, F., Fulchignoni, M., Ghafoor,
537 N.A.L., Kargl, G., Svedhem, H., Delderfield, J., Grande, M., Parker, D.J., Challenor, P.G.
538 and Geake, J.E., 2005. A soft solid surface on Titan as revealed by the Huygens Surface
539 Science Package. *Nature* 438, 792-795.
- 540 Zou, R.P. and Yu, A.B. 1995. The packing of spheres in a cylindrical container: The thickness
541 effect. *Chem. Eng. Sci.* 50, 1504-1507.

542 **Figure captions**

543 Figure 1. Schematic of the SSP instrument showing the location of the penetrometer at the base
544 of the probe immediately behind the ablative heat shield. Dimensions of the penetrometer and the
545 approximate position of the Electromagnetic Compatibility (EMC) screen are shown. (Upper
546 Image credit James Garry)

547
548 Figure 2. ACC-E penetrometry signature returned from the surface of Titan calibrated and
549 processed into force against depth, including correction for the transfer function of the
550 electronics. No smoothing has been applied. The penetration analysis stages are marked.

551
552 Figure 3. Free fall drop rig arrangement and data acquisition equipment. For the purposes of
553 comparison with the flight data impact speed of 4.6 m s^{-1} , the drop height of the penetrometer
554 above the target surface was set to 1.07 m. Bottom: schematic diagram of signal and data
555 processing paths for the flight and laboratory data.

556
557 Figure 4. Illustration of the peak and trough finding algorithm. The search starts from the
558 beginning of target penetration and identifies candidate peaks and troughs. To be accepted each
559 candidate peak and trough must have a significant rise and fall on either side. The significance is
560 based on the standard deviation of the noise on the signal as the penetrometer falls prior to
561 impact.

562
563 Figure 5. Mean peak-to-trough force amplitude plotted against bead mass for 31 drops into plastic
564 and glass bead targets. Standard errors are marked when larger than the data point.

565

566 Figure 6. Equipment used to produce a moisture gradient in sand with minimum mechanical
567 disturbance using a siphon principle. Moisture content was measured prior to each drop using a
568 ThetaProbe inserted into the sides of the container. Sampling points were offset to minimise sand
569 disturbance.

570
571 Figure 7. Penetrometry signatures for dry RH T (fine grained) sand in two densities, achieved by
572 physical compaction of the target. Impact is at 4.6 m s^{-1} .

573
574 Figure 8. Penetrometer signature for dry LB (coarse grained) sand in loose and dense state
575 showing noticeably greater tip entry impact peaks than those seen in the finer RH T sand. Impact
576 speed is 4.6 m s^{-1} .

577
578 Figure 9. Penetrometer signature for RH T (fine grained) sand with water: (a) saturated sand
579 (water table height $z=350 \text{ mm}$) (b) water table at $z = 250 \text{ mm}$ (c) water table at $z = 200 \text{ mm}$ (d)
580 water table at $z = 150 \text{ mm}$.

581
582 Figure 10. Penetrometer signatures for wet LB (coarse grained) sand: (a) saturated sand (water
583 table height $z = 350 \text{ mm}$) (b) water table at $z = 250 \text{ mm}$ (c) water table at $z = 200 \text{ mm}$ (d) water
584 table at $z = 150 \text{ mm}$.

585
586 Figure 11. Penetrometer signature of a drop into loosely packed snow at Huygens impact speed.
587 The signature from the probe (grey) has also been plotted for comparison of the initial entry force
588 (arrowed). The snow signature indicates the variation in density with depth of the material
589 probably caused by packing it into the target container.

590
591 Figure 12. Penetrometry signature from Huygens overlaid on the closest analogue match for the
592 third stage (substrate) material, wet Leighton Buzzard coarse sand with a water table 150 mm
593 below the sand surface (i.e. $z=200$). The flight signature has been shifted horizontally (but not
594 rescaled) to align the third stage with the start of the analogue drop. Penetration speed in both
595 cases is 4.6 m s^{-1} .

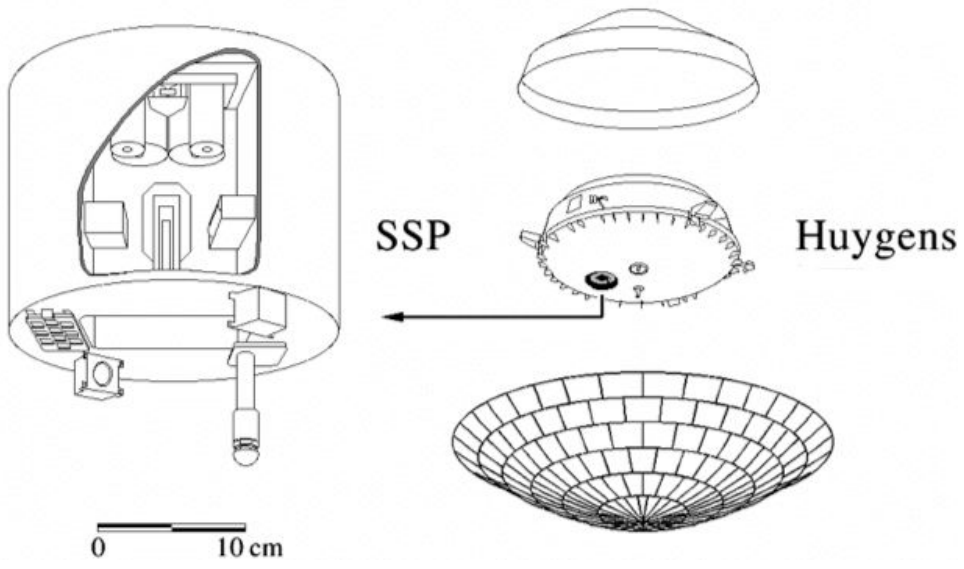
596
597 Figure 13. Surface material identification using two signature parameters. Parameters exclude the
598 first 1 cm 'tip entry' of signature for comparative purposes with the Huygens third stage of
599 signature. Where multiple drops of an analogue are available averages have been taken and
600 standard errors are shown. There is a marked difference between the flight data's signature
601 gradient compared to the terrestrial analogues.

602

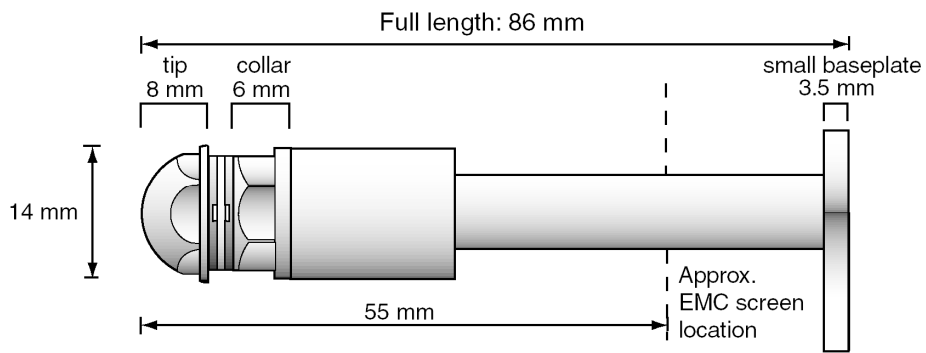
603 Figure 1

604

605



606

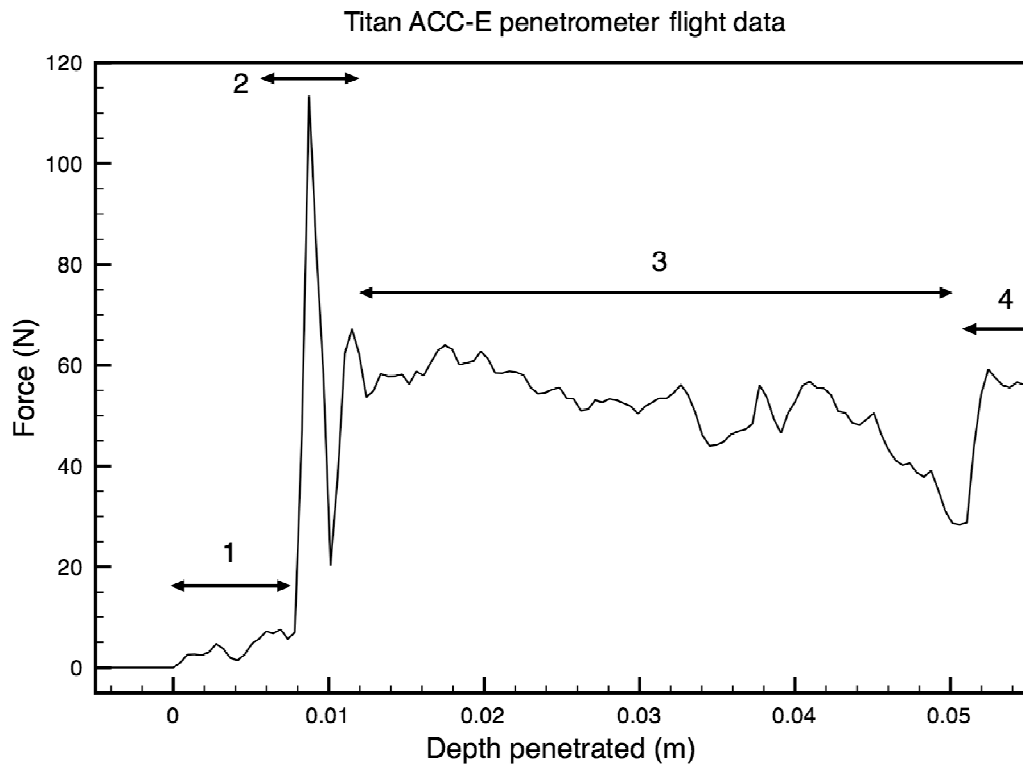


607

608

609 Figure 2

610

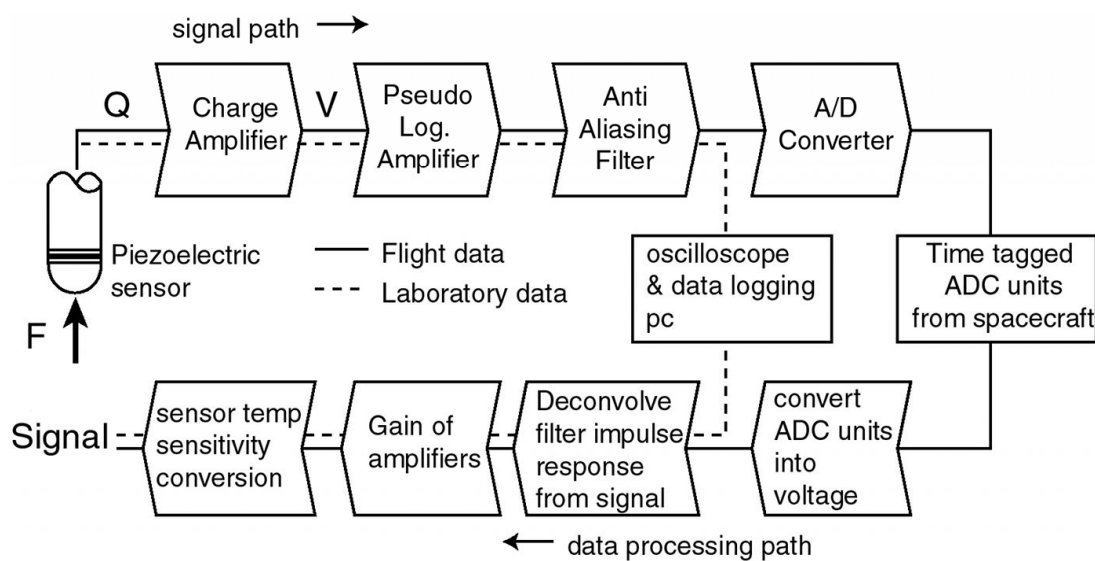
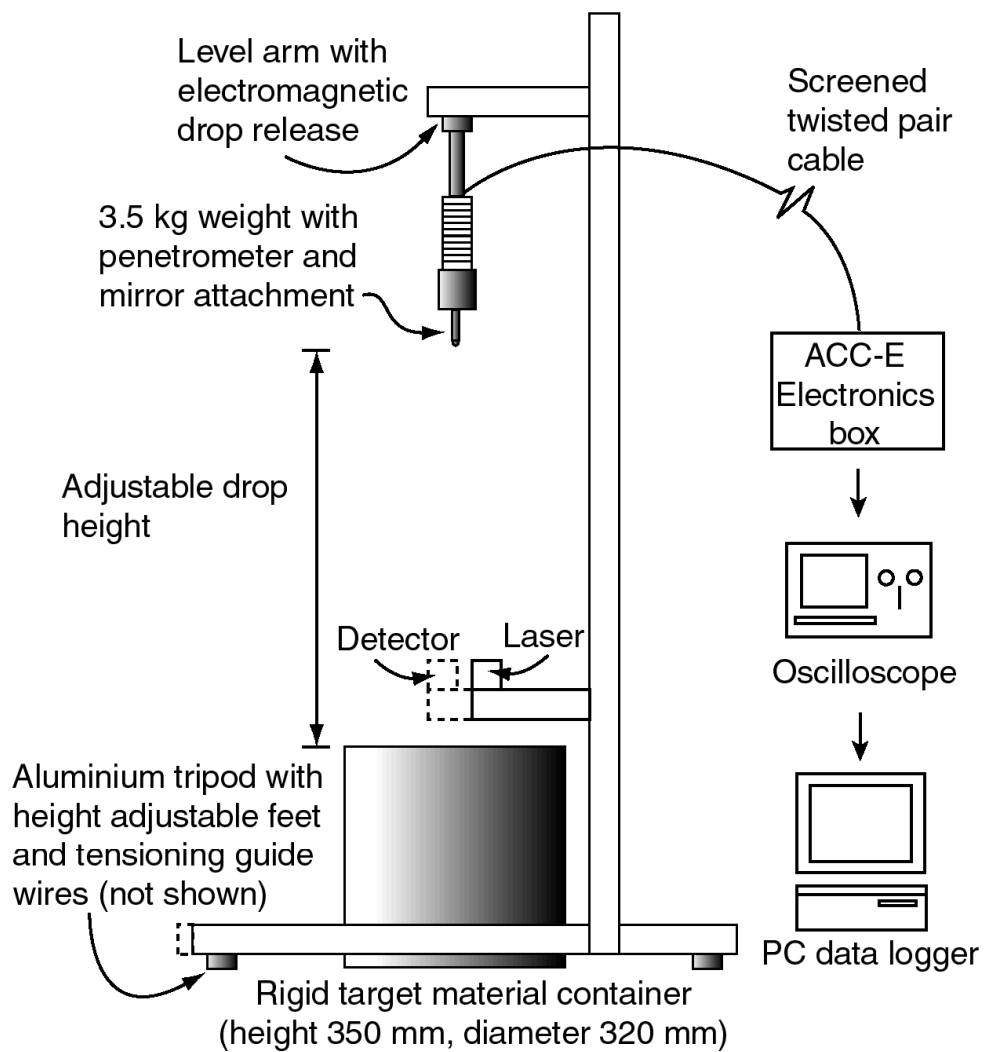


611

612

613

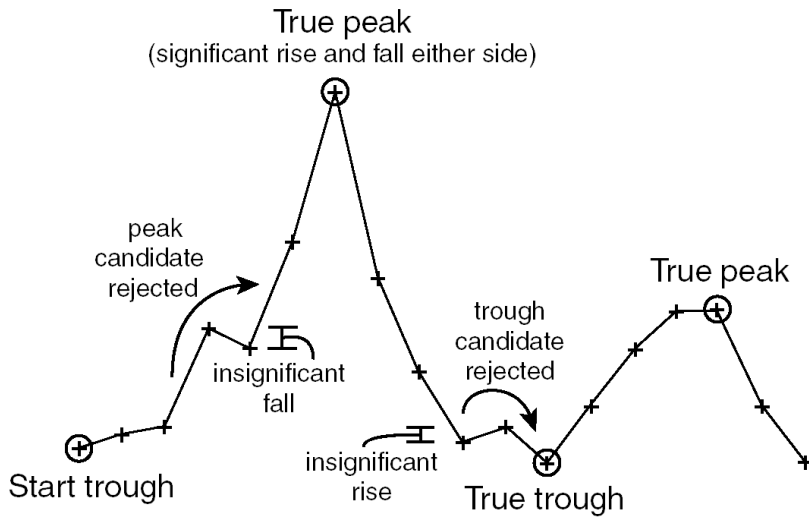
614 Figure 3



616 Figure 4

617

618



619

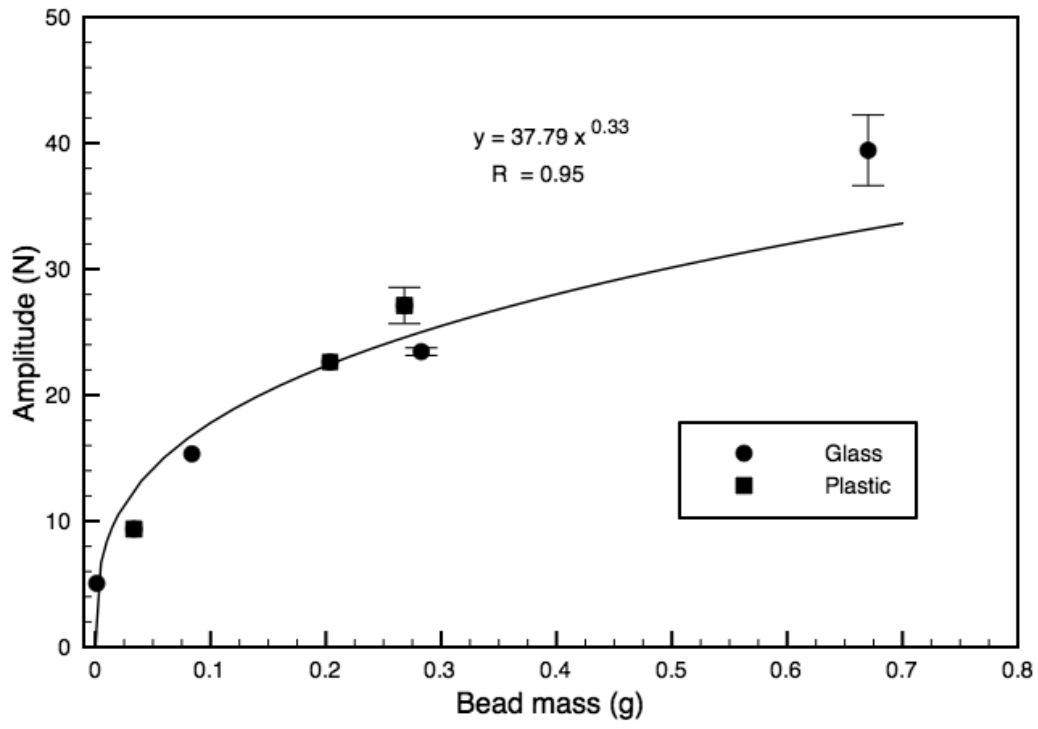
620

621 Figure 5

622

623

624



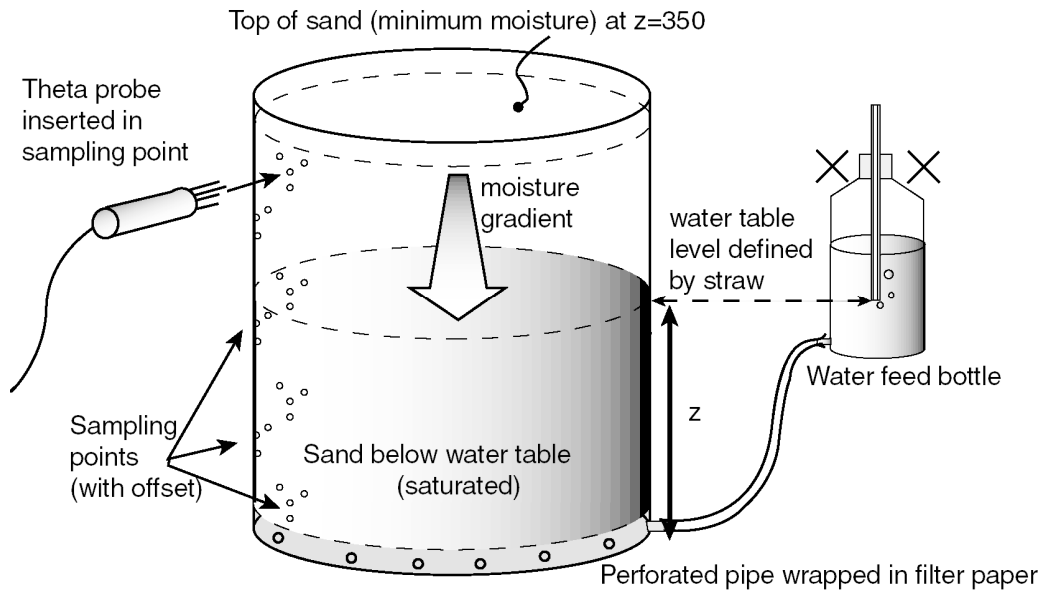
625

626

627 Figure 6

628

629



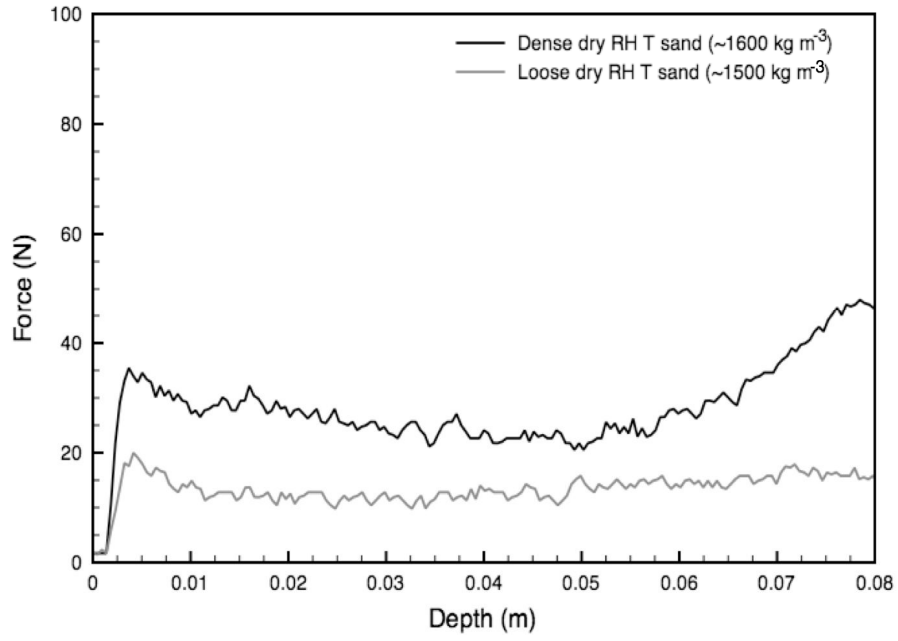
630

631

632 Figure 7

633

634



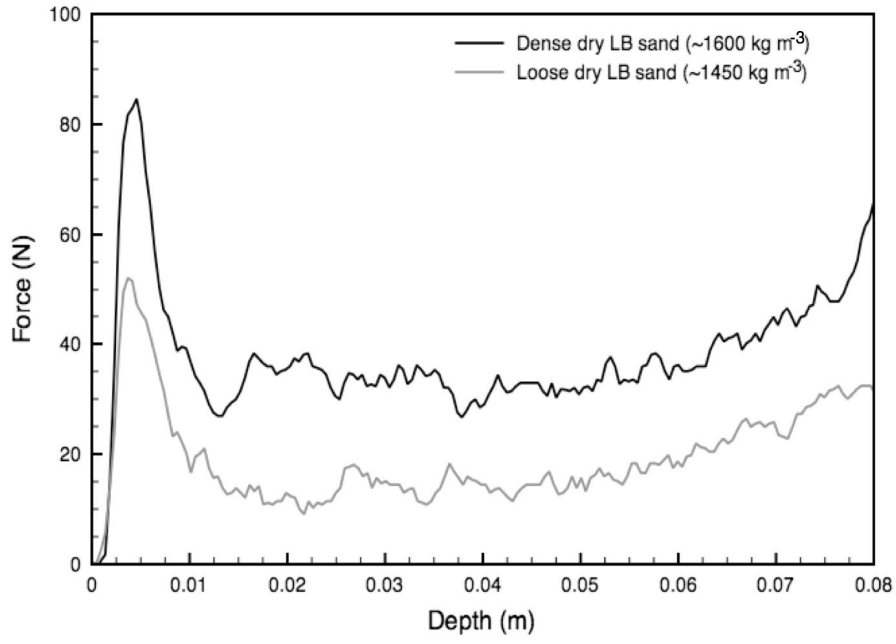
635

636

637 Figure 8

638

639



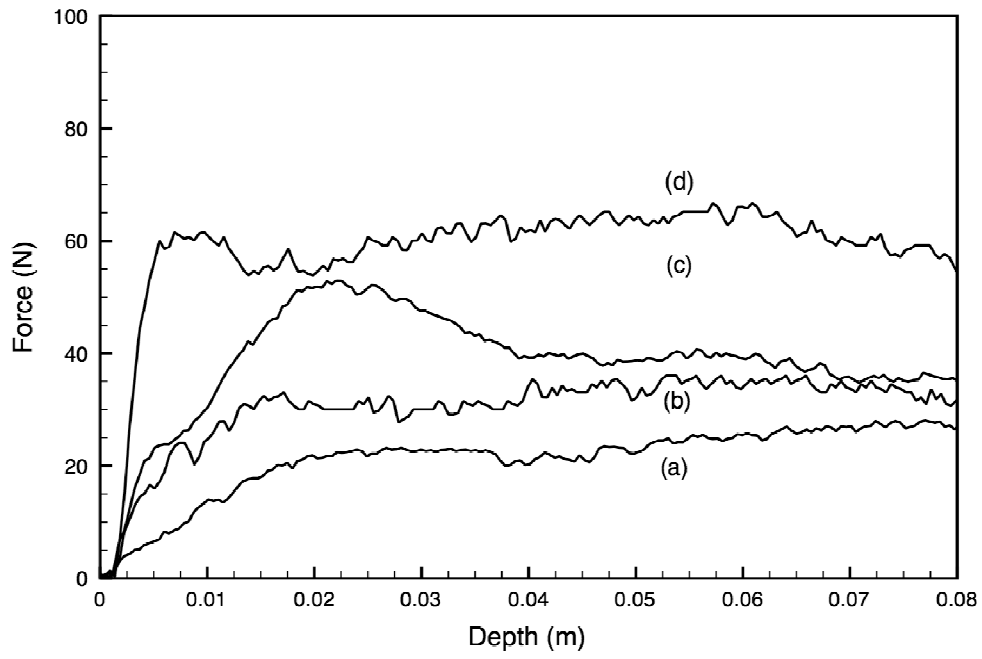
640

641

642 Figure 9

643

644



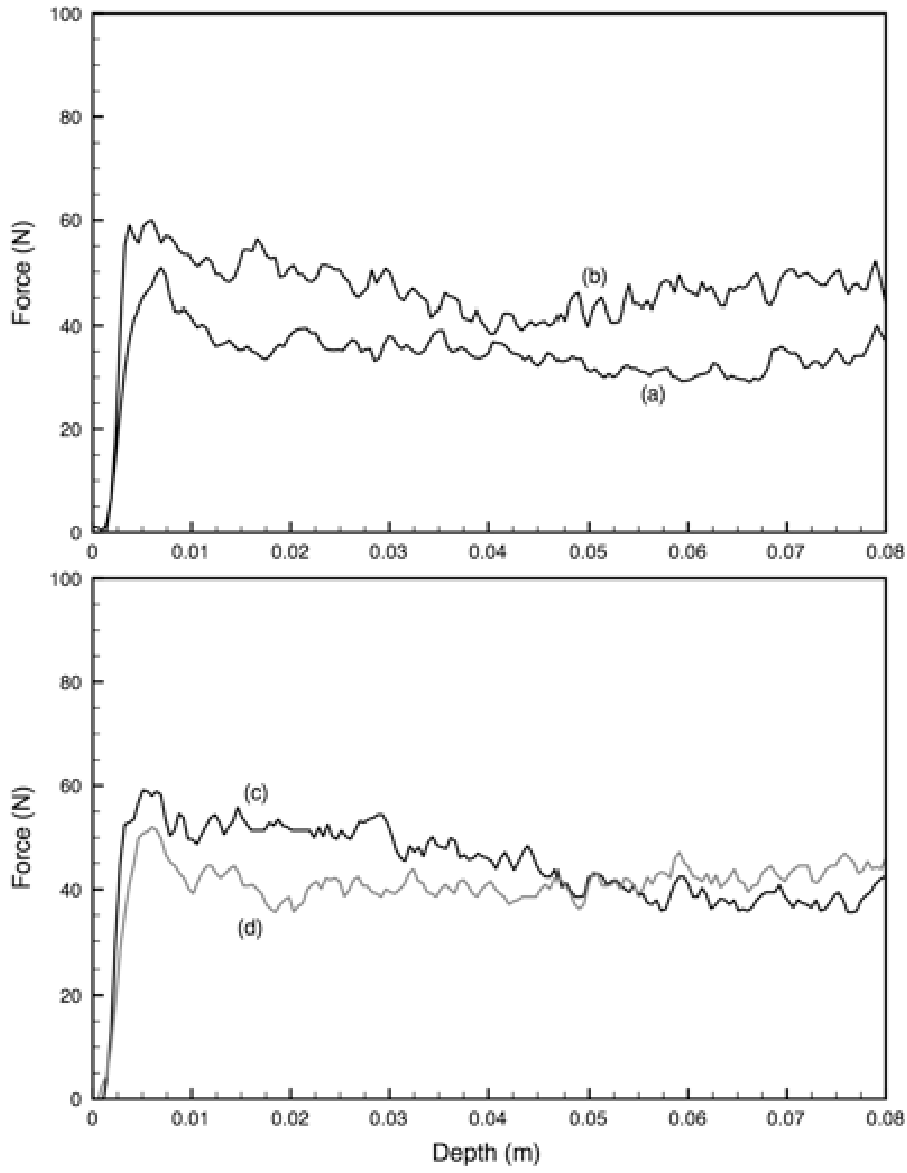
645

646

647 Figure 10

648

649



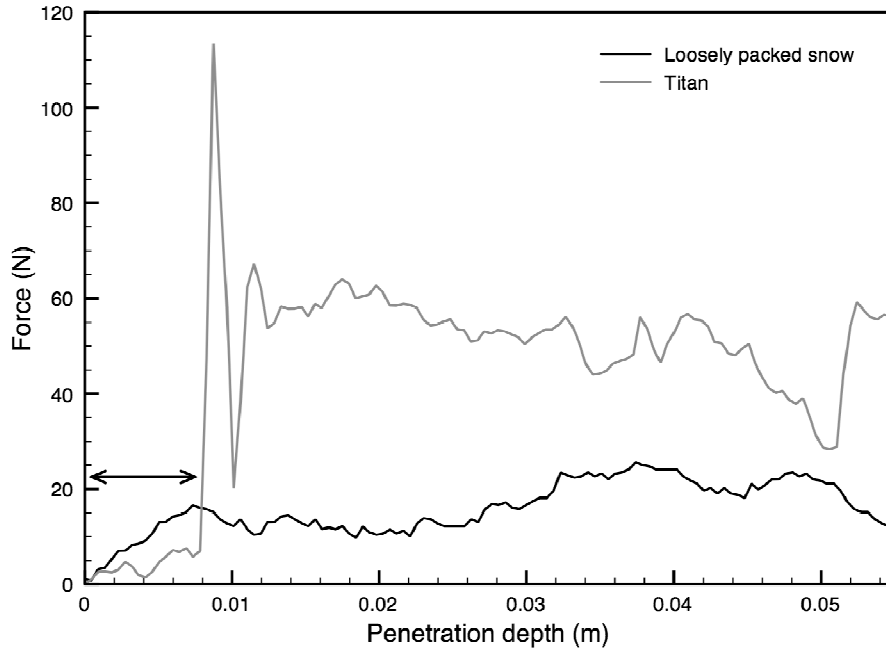
650

651

652 Figure 11

653

654



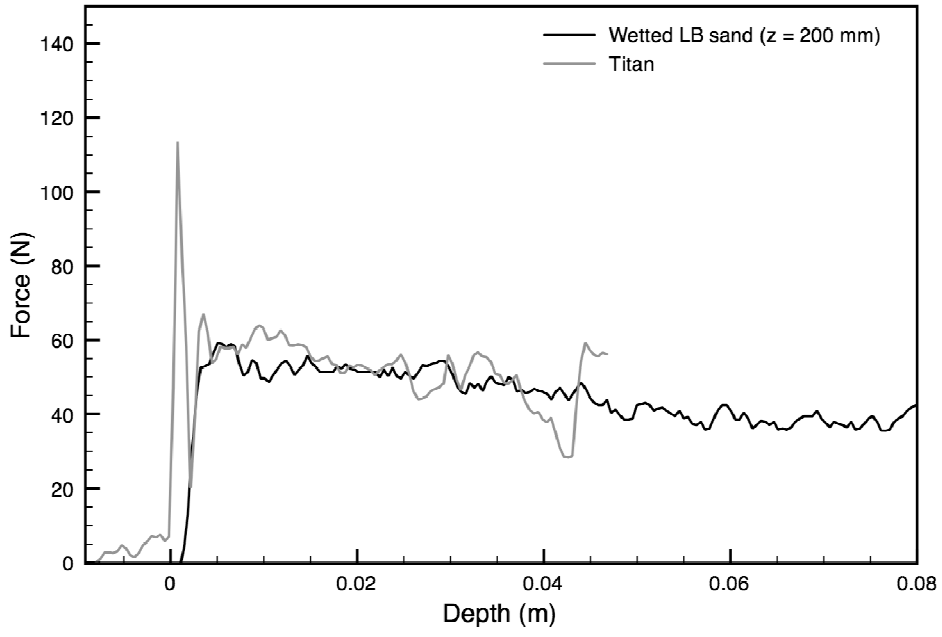
655

656

657 Figure 12

658

659



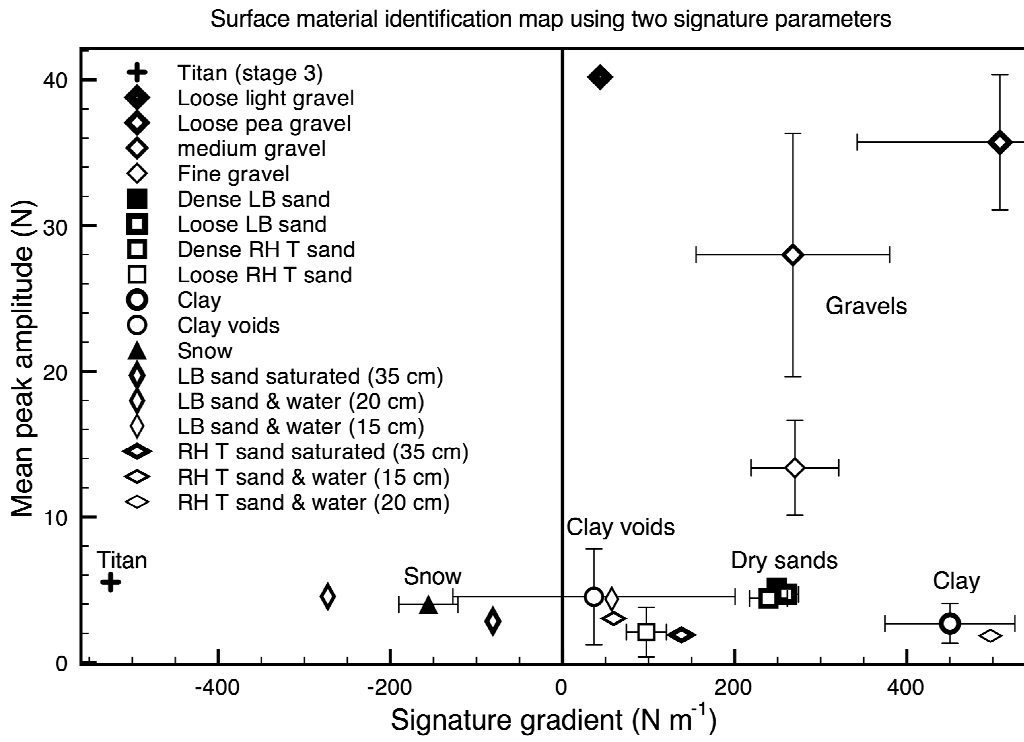
660

661

662 Figure 13

663

664



665

666

667

668